Improved Deadbeat Predictive Current Control of PMSM Drives With Repetitive Control-Based Disturbance Correction Observer

Haiyang Cao, *Graduate Student Member, IEEE*, Yongting Deng, *Senior Member, IEEE*, Jing Liu, *Member, IEEE*, Yun Zuo, *Graduate Student Member, IEEE*, Xiufeng Liu, *Student Member, IEEE*, Huanzhi Wang, *Graduate Student Member, IEEE*, and Christopher H. T. Lee, *Senior Member, IEEE*

***Abstract*—In order to achieve high robustness and high-precision current control, this article proposes a disturbance correction observer based on repetitive control (RDCO) for deadbeat predictive current control (DPCC-RDCO) scheme of permanent magnet synchronous motor (PMSM). In this technology, the disturbance correction based on the disturbance estimation of the extended state observer is presented to enhance the observer robustness. Meanwhile, a repetitive controller is embedded into the disturbance correction term to improve the estimation accuracy of periodic harmonics. Furthermore, the estimation performance, parameter characteristics, and convergence stability of the proposed observer are theoretically analyzed. With the current disturbance and current prediction accurately estimated by the RDCO, the improved DPCC scheme based on the established predictive current model is developed. Compared with the basic schemes, the proposed DPCC-RDCO can effectively suppress current deviation, and achieve excellent dynamic tracking and robust performance. Finally, the effectiveness and superiority of the studied method are verified experimentally in PMSM drives under different operating conditions.**

***Index Terms*—Deadbeat predictive current control (DPCC), disturbance correction observer, permanent magnet synchronous motor (PMSM), repetitive control.**

Received 6 May 2024; revised 7 July 2024 and 22 August 2024; accepted 13 October 2024. Date of publication 17 October 2024; date of current version 12 December 2024. This work was supported in part by the National Nature Science Foundation of China under Grant 12122304, Grant 12473083, and Grant 12303085, in part by Jilin Province Key R&D Plan Project under Grant 20220203036SF, in part by Jilin Province Science and Technology Innovation Platform Project under Grant 20230505007ZP, in part by Youth Innovation Promotion Association CAS under Grant Y2023060, and in part by Jilin Province Science and Technology Development Project under Grant 20240302044GX and Grant 20230203113SF. Recommended for publication by Associate Editor Michael Hartmann. *(Corresponding author: Yongting Deng.)*

Haiyang Cao and Xiufeng Liu are with the Changchun Institute of Optics, Fine Mechanics, and Physics, Chinese Academy of Sciences, Changchun 130033, China, and also with the University of Chinese Academy of Sciences, Beijing 100049, China (e-mail: caohaiyang20@mails.ucas.ac.cn; liuxiufeng20@mails.ucas.ac.cn).

Yongting Deng and Jing Liu are with the Changchun Institute of Optics, Fine Mechanics, and Physics, Chinese Academy of Sciences, Changchun 130033, China (e-mail: dengyongting@ciomp.ac.cn; liujing@ciomp.ac.cn).

Yun Zuo is with the Ministry of Education Key Laboratory of Magnetic Suspension Technology and Maglev Vehicle, Southwest Jiaotong University, Chengdu 610031, China (e-mail: z_uoy_un@my.swjtu.edu.cn).

Huanzhi Wang and Christopher H. T. Lee are with the School of Electrical and Electronic Engineering, Nanyang Technological University, Singapore, Singapore 639798 (e-mail: huanzhi001@e.ntu.edu.sg; chtlee@ntu.edu.sg).

Color versions of one or more figures in this article are available at https://doi.org/10.1109/TPEL.2024.3482315.

Digital Object Identifier 10.1109/TPEL.2024.3482315

I. Introduction

IN ELECTRIC drives, there is an increasing demand for high-precision and high-dynamic current control of permanent magnet synchronous motor (PMSM), especially in high-performance servosystems such as high-positioning turntables and high-direction large-aperture telescopes [1], [2], [3]. Therefore, in order to achieve the current with high accuracy and fast response, many scholars have investigated many intensive control strategies for the current loop, such as sliding mode control [4], active disturbance rejection control [5], and predictive current control (PCC) [6], and so on.

Among these advanced algorithms, the PCC method stands out as a potential scheme for precise current control due to its high dynamic response and compatibility with digital control system [7]. The PCC scheme can be divided into two categories based on the existence of space vector modulation: finite control set PCC without the modulator and continuous control set PCC with the modulator. Deadbeat PCC (DPCC) is regarded as an effective control strategy of continuous control set with space vector modulation based on the current predictive model [8]. However, in the practical implementation, DPCC has two key issues that need to be solved. The first is the inherent delay in the reference voltage calculation and implementation, which deteriorates the control performance. Fortunately, the delay problem can be eliminated by one-step forward prediction [9]. The other issue is that due to the high dependence of DPCC on system model [10], it is vulnerable to unmodeled disturbances in PMSM systems, including model mismatch [11], periodic harmonics caused by deadtime effect and flux harmonics [12]. Thus, it is essential to enhance the robustness of the prediction model to improve the accuracy of deadbeat control.

In recent years, the predictive control combined with various disturbance observers has become a promising scheme to achieve excellent robustness, such as Luenberger observer [13], extended state observer (ESO) [14], sliding-mode observer (SMO) [15]. In [8], a DPCC method with adaptive SMO based on a novel exponential reaching law is presented to optimize the current control performance. Yu et al. [16] proposed a composite observer based on SMO and generalized proportional-integral observer (GPIO) to inherit the advantages of high dynamics and disturbance suppression. In addition, some novel

structures of observers are demonstrated to improve the current prediction accuracy and reduce the current tracking error. For example, an enhanced observer based on a prediction error model is investigated in [17] to achieve both current prediction and disturbance estimation, a parallel observer is designed to achieve accurate current prediction in [18], and a hybrid ESO structure is developed to suppress prediction control noise [19]. Furthermore, the adaptive and nonlinear methods are studied to further enhance the observer robustness, such as exponential ESO [20], adaptive full-order observer [21], and adaptive flux observer [22]. Although these DPCC techniques with enhanced observers can improve dynamic performance and robustness to parameter mismatch, the current periodic harmonics are not eliminated, which may cause intolerable mechanical vibrations. Hence, it is necessary to further investigate the strategies of periodic disturbance suppression in predictive current control theory.

At present, the methods based on internal model control are the mainstream of research on current harmonic suppression in predictive current control, which include resonant control [23], iterative learning [24], and repetitive control [25]. In [24], an enhanced DPCC with iterative SMO is presented to improve the current control accuracy of PMSM. Tian et al. [25] combined the repetitive control with the active disturbance rejection in parallel in the discrete domain to attenuate the current disturbances. Song et al. [26] proposed a predictive vector-resonant current control based on ESO to eliminate the model mismatch and periodic disturbances. However, the resonant control requires multiple parallel connections to suppress multiple harmonics, which may make the system unstable and parameter tuning difficult [27]. Besides, the iterative learning control increases the computational burden. Thus, the repetitive control is a promising candidate to deal with multiple harmonic components of periodic disturbances.

To improve the robustness of the observer technique and achieve high-precision current control, this article proposes an improved DPCC scheme with repetitive control-based disturbance correction observer (RDCO). Compared with the existing DPCC schemes, the main contributions of the proposed method are summarized as follows.

1) The correction term of the disturbance estimation based on the ESO is proposed to enhance the disturbance robustness, thereby forming the disturbance correction observer (DCO).
2) A novel structure of RDCO is proposed, which introduces repetitive control in the correction term of the designed DCO to handle harmonics. The disturbance estimation, parameter characteristics, and stability of the RDCO are analyzed.
3) The proposed DPCC-RDCO features aperiodic and periodic disturbance estimation, current prediction and deadbeat control, and its superiority is validated by experiments.

The rest of this article is organized as follows. In Section II, the dynamic model, conventional DPCC, and disturbance analysis are presented. In Section III, the proposed DPCC scheme with RDCO is designed and the performance is theoretically analyzed. In Section IV, the experimental comparisons are presented to verify the performance of the studied method. Finally, Section V concludes this article.

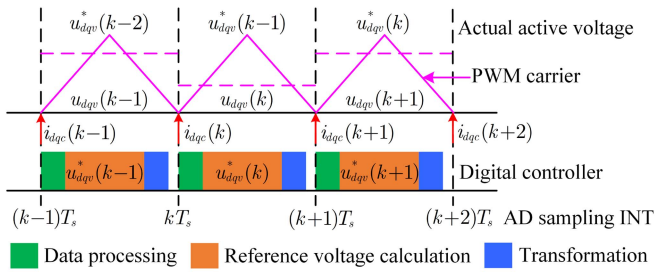

Fig. 1. Schematic diagram of the digital system control timing sequence.

II. Problem Formulation

A. Mathematical Model of PMSM Drives

Assuming that the three-phase winding structure of the employed PMSM is symmetrical and the eddy current losses and magnetic saturation are negligible, the ideal mathematical model of the stator current in the dq synchronous rotating frame can be presented as

$$\frac{d}{dt}\begin{bmatrix} i_{dc} \\ i_{qc} \end{bmatrix} = \begin{bmatrix} -R_s/L_{sd} & \omega_e L_{sq}/L_{sd} \\ -\omega_e L_{sd}/L_{sq} & -R_s/L_{sq} \end{bmatrix}\begin{bmatrix} i_{dc} \\ i_{qc} \end{bmatrix} + \begin{bmatrix} 1/L_{sd} & 0 \\ 0 & 1/L_{sq} \end{bmatrix}\begin{bmatrix} u_{dv} \\ u_{qv} \end{bmatrix} + \begin{bmatrix} 0 \\ -\psi_f \omega_e / L_{sq} \end{bmatrix} \quad (1)$$

where i_{dc} and u_{dv} represent the d-axis stator current and voltage, respectively; i_{qc} and u_{qv} represent the q-axis stator current and voltage, respectively; R_s and ψ_f denote the stator resistance and permanent magnet flux, respectively; ω_e is the electrical angular speed; L_{sd} and L_{sq} stand for the stator inductances of the dq-axis, respectively. Specifically, the subsequent analysis employs a surface-mounted PMSM, where $L_{sd} = L_{sq} = L_s$.

The sampling time T_s of the current loop is usually small enough, then at the k sampling instant, the equivalent discrete current model of PMSM based on 1) utilizing the zero-order hold method is described as

$$\begin{bmatrix} i_{dc}(k+1) \\ i_{qc}(k+1) \end{bmatrix} = H(k)\begin{bmatrix} i_{dc}(k) \\ i_{qc}(k) \end{bmatrix} + P\begin{bmatrix} u_{dv}(k) \\ u_{qv}(k) \end{bmatrix} + M(k) \quad (2)$$

where

$$H(k) = \begin{bmatrix} 1 - R_s T_s/L_s & \omega_e(k) T_s \\ -\omega_e(k) T_s & 1 - R_s T_s/L_s \end{bmatrix}$$

$$P = \begin{bmatrix} T_s/L_s & 0 \\ 0 & T_s/L_s \end{bmatrix}, M(k) = \begin{bmatrix} 0 \\ -\omega_e(k) T_s \psi_f / L_s \end{bmatrix}.$$

B. Conventional Deadbeat Predictive Current Control

Due to the PWM implementation of the digital control system as presented in Fig. 1, the one-sampling period delay between

the reference voltage u^*_{dqv} calculated at the k instant and the actual active voltage u_{dqv} employed at the $k+1$ instant is not considered under the conventional DPCC framework. The one-step delay can be modeled as

$$\begin{bmatrix} u^*_{dv}(k) \\ u^*_{qv}(k) \end{bmatrix} = \begin{bmatrix} u_{dv}(k+1) \\ u_{dv}(k+1) \end{bmatrix}. \tag{3}$$

Then, taking into account the one-step delay, the reference voltage at the k instant can be calculated from the states at the $k+1$ instant and $k+2$ instant, which can be derived as

$$\begin{bmatrix} u^*_{dv}(k) \\ u^*_{qv}(k) \end{bmatrix} = \hat{P}^{-1} \left\{ \begin{bmatrix} i_{dc}(k+2) \\ i_{qc}(k+2) \end{bmatrix} - \hat{H}(k) \begin{bmatrix} i_{dc}(k+1) \\ i_{qc}(k+1) \end{bmatrix} - \hat{M}(k) \right\} \tag{4}$$

where $\hat{H}(k)$, $\hat{P}$, and $\hat{M}(k)$ are the given parameters for the controller, including nominal values $\hat{R}_s$, $\hat{\psi}_f$, and $\hat{L}_s$. $\omega_e(k+1)$ is approximate to $\omega_e(k)$ under sufficiently small T_s. According to the discrete model at the k instant, the dq-axis currents at the $k+1$ instant in (4) can be predicted as

$$\begin{bmatrix} \hat{i}_{dc}(k+1) \\ \hat{i}_{qc}(k+1) \end{bmatrix} = \hat{H}(k) \begin{bmatrix} i_{dc}(k) \\ i_{qc}(k) \end{bmatrix} + \hat{P} \begin{bmatrix} u^*_{dv}(k-1) \\ u^*_{qv}(k-1) \end{bmatrix} + \hat{M}(k). \tag{5}$$

Substituting (5) into (4), and the actual current vector after two modulation periods is close to the reference currents, then the control voltages with one-step delay compensation in conventional DPCC scheme can be constructed as

$$\begin{bmatrix} u^*_{dv}(k) \\ u^*_{qv}(k) \end{bmatrix} = \hat{P}^{-1} \left\{ \begin{bmatrix} i^*_{dc}(k+2) \\ i^*_{qc}(k+2) \end{bmatrix} - \hat{H}(k) \begin{bmatrix} \hat{i}_{dc}(k+1) \\ \hat{i}_{qc}(k+1) \end{bmatrix} - \hat{M}(k) \right\}. \tag{6}$$

C. Disturbance Analysis

In the DPCC framework, the control performance is closely related to the accuracy of the model of the electrical motor. However, the PMSM deadbeat control system inevitably suffers from aperiodoc disturbance introduced by model mismatch and unmodeled dynamics, periodic disturbance caused by flux harmonics and inverter nonlinearity. These disturbances usually result in current steady-state error and current harmonics. Thus, it is essential to consider these various disturbances when constructing the DPCC.

Defining vector $\boldsymbol{x} = \begin{bmatrix} i_{dc} & i_{qc} \end{bmatrix}^T$ and $\boldsymbol{u} = \begin{bmatrix} u_{dv} & u_{qv} \end{bmatrix}^T$, the state-space realization of the model can be expressed as

$$\begin{aligned} \dot{\boldsymbol{x}} &= \boldsymbol{A}\boldsymbol{x} + \boldsymbol{B}\boldsymbol{u} + \boldsymbol{D} \\ &\quad + \underbrace{\Delta\boldsymbol{A}\boldsymbol{x} + \Delta\boldsymbol{B}\boldsymbol{u} + \Delta\boldsymbol{D} + \boldsymbol{\xi}}_{\boldsymbol{f_a}} + \underbrace{\boldsymbol{B}(\Delta\boldsymbol{u} + \omega_e\boldsymbol{\psi_h})}_{\boldsymbol{f_p}} \end{aligned} \tag{7}$$

and

$$\begin{cases} \boldsymbol{A} = \begin{bmatrix} -\hat{R}_s/\hat{L}_s & \omega_e \\ -\omega_e & -\hat{R}_s/\hat{L}_s \end{bmatrix}, \boldsymbol{B} = \begin{bmatrix} 1/\hat{L}_s & 0 \\ 0 & 1/\hat{L}_s \end{bmatrix} \\ \boldsymbol{D} = \begin{bmatrix} 0 \\ -\omega_e\hat{\psi}_f/\hat{L}_s \end{bmatrix}, \boldsymbol{\xi} = \begin{bmatrix} \xi_d \\ \xi_q \end{bmatrix}, \Delta\boldsymbol{u} = \begin{bmatrix} \Delta u_d \\ \Delta u_q \end{bmatrix} \end{cases} \tag{8}$$

where Δ represents the corresponding parameter variation, $\boldsymbol{\xi}$ denotes the dq-axis unmodeled dynamics, $\Delta\boldsymbol{u}$ is the dq-axis voltage harmonics due to inverter nonlinearity, $\boldsymbol{\psi_h}$ is the dq-axis flux harmonics; $\boldsymbol{f_a}$ and $\boldsymbol{f_p}$ represent aperiodic disturbance and periodic disturbance, respectively, and their sum denotes the lumped disturbance $\boldsymbol{f}$, i.e., $\boldsymbol{f} = \boldsymbol{f_a} + \boldsymbol{f_p}$. The projection of the aperiodic disturbance on the dq axis is $\boldsymbol{f_a} = \begin{bmatrix} f_{ad} & f_{aq} \end{bmatrix}^T$, which can be specifically given as

$$\begin{cases} f_{ad} = \frac{\hat{R}_s\Delta L_{sd} - \Delta R_s\hat{L}_s}{\hat{L}_s(\hat{L}_s+\Delta L_{sd})} i_{dc} - \frac{\Delta L_{sd}}{\hat{L}_s(\hat{L}_s+\Delta L_{sd})} u_{dv} \\ \qquad + \frac{\omega_e(\Delta L_{sq} - \Delta L_{sd})}{\hat{L}_s + \Delta L_{sd}} i_{qc} + \xi_d \\ f_{aq} = \frac{\hat{R}_s\Delta L_{sq} - \Delta R_s\hat{L}_s}{\hat{L}_s(\hat{L}_s+\Delta L_{sq})} i_{qc} - \frac{\Delta L_{sq}}{\hat{L}_s(\hat{L}_s+\Delta L_{sq})} u_{qv} \\ \qquad - \frac{\omega_e(\Delta L_{sd} - \Delta L_{sq})}{\hat{L}_s + \Delta L_{sq}} i_{dc} + \frac{\psi_f\Delta L_{sq} - \Delta\psi_f\hat{L}_s}{\hat{L}_s(\hat{L}_s+\Delta L_{sq})}\omega_e + \xi_q \end{cases} \tag{9}$$

where $\Delta R_s = R_s - \hat{R}_s$, $\Delta\psi_f = \psi_f - \hat{\psi}_f$; $\Delta L_{sd} = L_{sd} - \hat{L}_s$, and $\Delta L_{sq} = L_{sq} - \hat{L}_s$ mean that the d- and q-axis inductance of the surface-mounted PMSM may vary inconsistently.

Besides, from [25] and [28], $\Delta\boldsymbol{u}$ and $\boldsymbol{\psi_h}$ can be modeled as

$$\begin{cases} \Delta\boldsymbol{u} = \begin{bmatrix} \Delta u_d \\ \Delta u_q \end{bmatrix} = \begin{bmatrix} \frac{4T_dU_{dc}}{\pi T_s} \sum_{k=1}^{\infty} \left[\frac{12k}{36k^2-1} \sin(6k\omega_e t) \right] \\ \frac{4T_dU_{dc}}{\pi T_s} \left\{ \sum_{k=1}^{\infty} \left[\frac{2}{36k^2-1} \cos(6k\omega_e t) \right] - 1 \right\} \end{bmatrix} \\ \boldsymbol{\psi_h} = \begin{bmatrix} \psi_{qh} \\ -\psi_{dh} \end{bmatrix} = \begin{bmatrix} \sum_{k=1}^{\infty} \psi_{q6kh} \sin(6k\omega_e t) \\ -\sum_{k=1}^{\infty} \psi_{d6kh} \cos(6k\omega_e t) \end{bmatrix} \end{cases} \tag{10}$$

where T_d, U_{dc}, and k are the dead time, dc-bus voltage, and positive integer, respectively; ψ_{d6kh} and ψ_{q6kh} denote the dq-axis magnitude of $6k$th flux harmonics, respectively. From (10), the inverter nonlinearity and flux harmonics will cause $6k$th periodic fluctuations in the dq-axis current.

III. Proposed RDCO-Based DPCC Scheme

To suppress the adverse effect of the aforementioned parameter mismatch and current harmonics, an improved deadbeat control strategy with a roust enhanced disturbance correction observer based on repetitive control is proposed in this section. The details of the proposed strategy are presented as following.

A. Design of RDCO

The proposed RDCO is developed on the basis of conventional ESO, in which the correction of disturbance estimation is added to enhance observer robustness and a repetitive controller is embedded into the disturbance correction term to deal with harmonic disturbances.

As aforementioned in Section II-C, in order to accurately observe the harmonic disturbances resulting from flux harmonics and inverter nonlinearity, a repetitive controller is introduced and formulated in the continuous-time domain as

$$G_{rc}(s) = \frac{K_{rc}e^{-sTN}}{1 - Q(s)e^{-sTN}} e^{sTK} \tag{11}$$

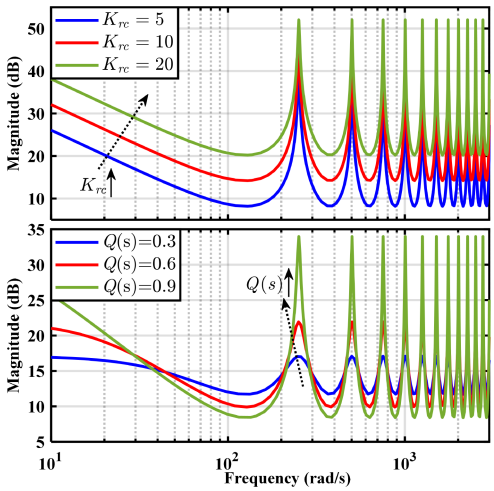

Fig. 2. Bode plots of the repetitive controller under different parameters.

where K_{rc} is the control gain, $Q(s)$ is normally chosen as a constant with amplitude less than 1 [25], e^{sTK} denotes the phase-lead compensator, e^{-sTN} is the delay link, $N = T_h/T_s$, $T_h = 2\pi/\omega_h$, and ω_h is the harmonic frequency and it need to be selected as $\omega_h = 6\omega_e$ to calculate the N in real time.

The bode plots of the repetitive controller are presented in Fig. 2. It can be seen that there are some large gains at the integer multiple frequencies of ω_h, while at other frequencies the amplitude decreases. In addition, a larger K_{rc} and $Q(s)$ have better harmonic elimination capability, but the selection of their specific values should be weighed with the stability consideration in the practical system.

Then, a novel RDCO from (7) with the disturbance correction term based on the repetitive controller is proposed as

$$\begin{cases} \dot{\hat{\boldsymbol{x}}} = \boldsymbol{A}\boldsymbol{x} + \boldsymbol{B}\boldsymbol{u} + \boldsymbol{D} + \hat{\boldsymbol{f}} - \gamma_1(\hat{\boldsymbol{x}} - \boldsymbol{x}) \\ \dot{\boldsymbol{z}} = -\gamma_2(\hat{\boldsymbol{x}} - \boldsymbol{x}) \\ \dot{\hat{\boldsymbol{f}}} = \left[\dot{G}_{rc}(t) + \frac{\gamma_2}{\alpha}\right](\boldsymbol{x} - \hat{\boldsymbol{x}}) - \frac{\omega_o(1-\alpha)}{2\alpha}(\hat{\boldsymbol{f}} - \boldsymbol{z}) \end{cases} \tag{12}$$

where $G_{rc}(t)$ is the expression of $G_{rc}(s)$ in the time domain, $\hat{\boldsymbol{x}}$ denotes the vector of dq-axis current estimation, which can be expressed as $\boldsymbol{x} = [\hat{i}_{dc} \;\; \hat{i}_{qc}]^T$, $\boldsymbol{z} = [z_d \;\; z_q]^T$ is the disturbance estimation vector before correction, $\hat{\boldsymbol{f}} = [\hat{f}_d \;\; \hat{f}_q]^T$ is the corrected lumped disturbance reconstruction vector. ω_o is the observer bandwidth, α is the disturbance correction factor, which ranges from 0 to 1. γ_1 and γ_2 are the observer gains, which from the pole configuration [29] are employed as

$$\gamma_i = \frac{2!}{(2-i)!i!}\omega_o^i, i = 1, 2. \tag{13}$$

Remark 1: It should be noted that the proposed RDCO is constructed by introducing the repetitive control of extracting periodic harmonics on the basis of the proposed DCO. Meanwhile, the DCO is also a novel observer proposed in this article, which is formed by designing a correction term with enhanced disturbance estimation on the basis of the conventional ESO. Fig. 3 shows three different observer structures formed by connecting three different terminals to terminal 4. The expression details of the conventional ESO and the proposed DCO are introduced in the Appendix.

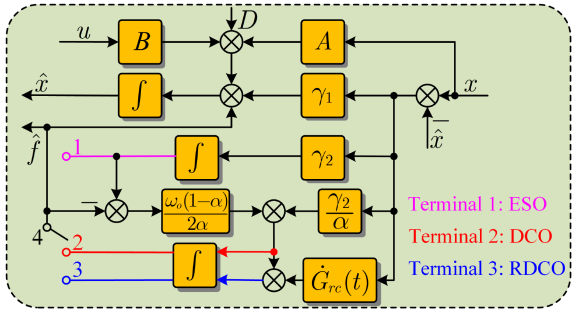

Fig. 3. Structures of the conventional ESO and the proposed DCO and RDCO.

B. Performance Analysis and Parameter Characteristics

In order to demonstrate that the proposed RDCO can better estimate low-frequency disturbance and periodic disturbance, this section conducts a comprehensive theoretical comparative analysis of the three observers in Fig. 3.

First, to evaluate the accuracy of disturbance estimation of the RDCO, according to (12) and (13), the transfer function of the proposed RDCO from the actual disturbance to the estimated disturbance, i.e., $\hat{F}(s)/F(s)$ can be derived as

$$\Phi_d^R(s) = \frac{2\alpha G_{rc}(s)s^2 + 2{\omega_o}^2 s + \omega_o^3 - \alpha\omega_o^3}{2\alpha s^3 + (\omega_o + 3\alpha\omega_o)s^2 + 2{\omega_o}^2 s + \omega_o^3 - \alpha\omega_o^3}. \tag{14}$$

Then, the transfer function from the actual disturbance to the disturbance estimation error, i.e., $[\hat{F}(s) - F(s)]/F(s)$ is

$$\Phi_e^R(s) = -\frac{2\alpha s^3 + [\omega_o + 3\alpha\omega_o - 2\alpha G_{rc}(s)]\, s^2}{2\alpha s^3 + (\omega_o + 3\alpha\omega_o)s^2 + 2{\omega_o}^2 s + \omega_o^3 - \alpha\omega_o^3}. \tag{15}$$

Similarly, based on (28) and (29) in the Appendix, the corresponding transfer function expressions of ESO and DCO are also given as follows

$$\begin{cases} \Phi_d^E(s) = \frac{{\omega_o}^2}{s^2 + 2\omega_o s + {\omega_o}^2}, \Phi_e^E(s) = \frac{-s^2 - 2\omega_o s}{s^2 + 2\omega_o s + {\omega_o}^2} \\ \Phi_d^D(s) = \frac{2{\omega_o}^2 s + \omega_o^3 - \alpha\omega_o^3}{2\alpha s^3 + (\omega_o + 3\alpha\omega_o)s^2 + 2{\omega_o}^2 s + \omega_o^3 - \alpha\omega_o^3} \\ \Phi_e^D(s) = -\frac{2\alpha s^3 + (\omega_o + 3\alpha\omega_o)s^2}{2\alpha s^3 + (\omega_o + 3\alpha\omega_o)s^2 + 2{\omega_o}^2 s + \omega_o^3 - \alpha\omega_o^3} \end{cases} \tag{16}$$

where $\Phi_d^E(s)$ and $\Phi_e^E(s)$ are the transfer functions of disturbance estimation and error of ESO; $\Phi_d^D(s)$ and $\Phi_e^D(s)$ are the transfer functions of disturbance estimation and error of DCO.

Obviously, when the disturbance is a step signal, three observers can estimate the step signal without error in the steady state. When the disturbance is a ramp signal with a slope of h, i.e., $F(s) = h/s^2$, the disturbance estimation errors based on the final value theorem can be obtained as

$$\begin{cases} \lim\limits_{t\to\infty} \Phi_e^E(t) f(t) = \lim\limits_{s\to 0} s\Phi_e^E(s)F(s) = -2h/\omega_o \\ \lim\limits_{t\to\infty} \Phi_e^D(t) f(t) = \lim\limits_{s\to 0} s\Phi_e^D(s)F(s) = 0 \\ \lim\limits_{t\to\infty} \Phi_e^R(t) f(t) = \lim\limits_{s\to 0} s\Phi_e^R(s)F(s) = 0. \end{cases} \tag{17}$$

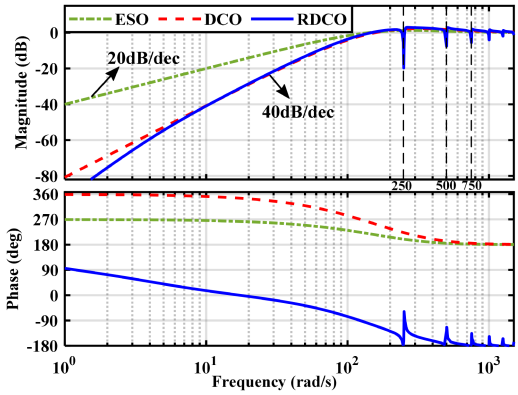

Fig. 4. Bode diagrams of $\Phi_e(s)$ for three different observers.

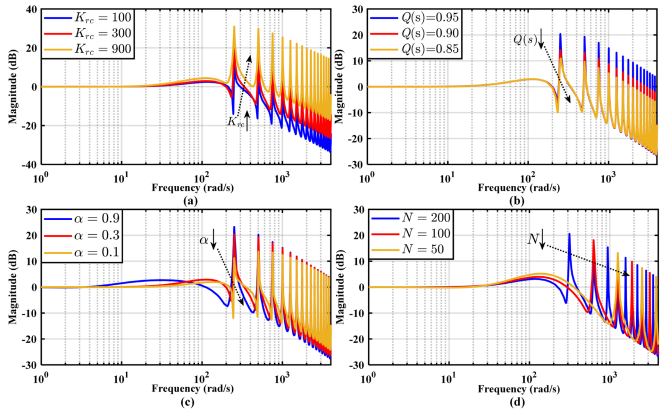

Fig. 5. Bode diagrams of $\Phi_d^R(s)$ under varying parameters.

Accordingly, the conventional ESO has a steady-state bias in estimating ramp disturbance, while the estimation errors of the proposed DCO and RDCO can converge to zero, which indicates that the DCO-based observers enhance robustness to various disturbances.

Furthermore, the Bode plots of the disturbance estimation error characteristics of three different observers under the same parameters $\omega_o = 200$, $\alpha = 0.4$, $K_{rc} = 30$, and $Q(s) = 0.9$ are shown in Fig. 4. It can be observed that at low frequencies, the slope of the amplitude curve of the conventional ESO is 20 dB/dec, and the slope of the amplitude of the presented DCO is 40 dB/dec, while the proposed RDCO exhibits an even higher slope, which indicates that the observers based on the proposed disturbance correction have better low-frequency disturbance rejection characteristics to enhance the estimation capability of slow-varying disturbance. In the mid-frequency band, the proposed RDCO and DCO amplitudes are consistent and have no amplitude higher than ESO, which means that the proposed disturbance-corrected observers possess the satisfactory dynamic estimation response. In addition, the RDCO appears a significant amplitude decrease to attenuate periodic harmonics at the integer multiple frequencies of ω_h. Therefore, the proposed RDCO can simultaneously improve the estimation performance of aperiodic and periodic disturbances.

The Bode diagrams of the disturbance estimation transfer function $\Phi_d^R(s)$ of RDCO with ω_o=200 under varying parameters are presented in Fig 5. The specific parameters are set as follows: $Q(s)$=0.95, α=0.3, and N=250 in Fig. 5(a), K_{rc}=300, α=0.3, and N=250 in Fig. 5(b), K_{rc}=300, $Q(s)$=0.95, and N=250 in Fig. 5(c), K_{rc}=300, $Q(s)$=0.95, and α=0.3 in Fig. 5(d). It can be noted from Fig. 5(a) that the amplitude at the harmonic frequency becomes larger with the increase of K_{rc}, which means that the estimation capability of harmonic disturbance is enhanced. Similarly, from Fig. 5(b), the effect of $Q(s)$ on the estimation of harmonic disturbance is consistent with changes in K_{rc}. In Fig. 5(c), with α decrease, the disturbance with larger bandwidths can be accurately estimated, which indicates that the decreasing α can improve the estimation ability of low-frequency disturbances, and the reduction of α also plays a little attenuating effect on the amplitude at the harmonic frequency. N can be configured according to the harmonic frequency to be suppressed, and from Fig. 5(d) that the proposed RDCO has a strong selection capability for periodic disturbance frequency. Thus, the proposed RDCO can effectively estimate disturbances by selecting appropriate parameters.

C. Stability and Convergence Analysis

Defining $\tilde{\boldsymbol{z}}_{\boldsymbol{i}} = \hat{\boldsymbol{z}}_{\boldsymbol{i}} - \boldsymbol{x}_{\boldsymbol{i}}$ as the estimation error of RDCO, where $i = 1, 2$, $\hat{\boldsymbol{z}}_{\boldsymbol{i}} = [\hat{\boldsymbol{x}}, \boldsymbol{z}]^T$, and $\boldsymbol{x}_{\boldsymbol{i}} = [\boldsymbol{x}, \boldsymbol{f}]^T$. Let $\eta_i = \tilde{z}_i/\omega_o^{j-1}$, where $j = 1, 2$, then the redefined observer estimation error can be presented as

$$\dot{\boldsymbol{\eta}} = \omega_o \boldsymbol{W}\boldsymbol{\eta} + \varphi \boldsymbol{L}/\omega_o \tag{18}$$

where φ is the first derivative of the lumped disturbance, and

$$\boldsymbol{\eta} = \begin{bmatrix} \eta_1 \\ \eta_2 \end{bmatrix}, \boldsymbol{W} = \begin{bmatrix} -2 & 1 \\ -1 & 0 \end{bmatrix}, \boldsymbol{L} = \begin{bmatrix} 0 \\ -1 \end{bmatrix}.$$

It can be easily deduced that both the eigenvalues of $\boldsymbol{W}$ are -1, $\boldsymbol{W}$ satisfies Hurwitz stable. Furthermore, a unique and symmetric positive definite matrix $\boldsymbol{G}$ exists and satisfies that

$$\boldsymbol{W}^{\boldsymbol{T}}\boldsymbol{G} + \boldsymbol{G}\boldsymbol{W} = -\boldsymbol{I} \tag{19}$$

where $\boldsymbol{G} = \begin{bmatrix} \frac{1}{2} & -\frac{1}{2} \\ -\frac{1}{2} & \frac{3}{2} \end{bmatrix}$. Choose $\boldsymbol{V}(\boldsymbol{\eta}) = \boldsymbol{\eta}^T\boldsymbol{G}\boldsymbol{\eta}$ as a Lyapunov function and taking derivative. Hence, it yields

$$\dot{V}(\boldsymbol{\eta}) = \dot{\boldsymbol{\eta}}^{\boldsymbol{T}}\boldsymbol{G}\boldsymbol{\eta} + \boldsymbol{\eta}^{\boldsymbol{T}}\boldsymbol{G}\dot{\boldsymbol{\eta}} = -\omega_o\|\boldsymbol{\eta}\|^2 + 2\omega_o^{-1}\boldsymbol{\eta}^{\boldsymbol{T}}\boldsymbol{G}\boldsymbol{L}\varphi. \tag{20}$$

Since φ is globally Lipschitz in terms of $\boldsymbol{x}$, that is, there exists a constant ρ such that $\varphi \le \rho\|\boldsymbol{x}_{\boldsymbol{i}} - \hat{\boldsymbol{z}}_{\boldsymbol{i}}\|$, it follows that

$$2\omega_o^{-1}\boldsymbol{\eta}^{\boldsymbol{T}}\boldsymbol{G}\boldsymbol{L}\varphi \le 2\rho\omega_o^{-1}\boldsymbol{\eta}^{\boldsymbol{T}}\boldsymbol{G}\boldsymbol{L}\|\boldsymbol{x}_{\boldsymbol{i}} - \hat{\boldsymbol{z}}_{\boldsymbol{i}}\|. \tag{21}$$

When $\omega_o \ge 1$, we get $\omega_o^{-1}\|\boldsymbol{x}_{\boldsymbol{i}} - \hat{\boldsymbol{z}}_{\boldsymbol{i}}\| = \omega_o^{-1}\|\tilde{\boldsymbol{z}}_{\boldsymbol{i}}\| \le \|\boldsymbol{\eta}\|$. Then, as given by

$$2\omega_o^{-1}\boldsymbol{\eta}^{\boldsymbol{T}}\boldsymbol{G}\boldsymbol{L}\varphi \le \lambda\|\boldsymbol{\eta}\|^2 \tag{22}$$

where $\lambda = \|\boldsymbol{G}\boldsymbol{L}\rho\|^2 + 1$. Substituting (22) into (20), we get

$$\dot{V}(\boldsymbol{\eta}) \le -(\omega_o - \lambda)\|\boldsymbol{\eta}\|^2 \tag{23}$$

that is, $\dot{V}(\boldsymbol{\eta}) < 0$ if $\omega_o > \lambda$. Thus, we obtain $\lim_{t\to\infty} \tilde{\boldsymbol{z}}_{\boldsymbol{i}} = 0$.

It can be noted that the Lyapunov asymptotic stability theorem holds. The analysis of the disturbance correction term is similar to the convergence of the second estimation term. Thus, when time tends to infinity, the estimation error of RDCO is zero. Based on the Lyapunov theory, the proposed observer is convergent in the engineering sense.

D. Implementation of Proposed DPCC Based on RDCO

The aforementioned design and analysis of the proposed RDCO are presented in the continuous domain. However, the proposed RDCO is only calculated at discrete instants and employed to the digital controller during the sampling interval. Considering that the current sampling time T_s is small enough in the discrete-time system, the aforementioned zero-order hold strategy is utilized to discretize the integrators.

Thus, based on (12), the discrete form of the proposed RDCO in the dq-axis can be obtained as

$$\begin{cases} \hat{i}_{dc}(k+1) = \hat{i}_{dc}(k) - \frac{T_s\hat{R}_s}{\hat{L}_s} i_{dc}(k) + T_s\omega_e(k) i_{qc}(k) \\ \quad + \frac{T_s}{\hat{L}_s} u_{dv}(k) + T_s\hat{f}_d(k) - T_s\gamma_1 \left[\hat{i}_{dc}(k) - i_{dc}(k)\right] \\ z_d(k+1) = z_d(k) - T_s\gamma_2 \left[\hat{i}_{dc}(k) - i_{dc}(k)\right] \\ \hat{f}_d(k+1) = \hat{f}_d(k) - \frac{\omega_o(1-\alpha)}{2\alpha} T_s \left[\hat{f}_d(k) - z_d(k)\right] \\ \quad + \left[G_{rc}(z) + T_s\frac{\gamma_2}{\alpha}\right] \left[i_{dc}(k) - \hat{i}_{dc}(k)\right] \end{cases} \tag{24}$$

$$\begin{cases} \hat{i}_{qc}(k+1) = \hat{i}_{qc}(k) - \frac{T_s\hat{R}_s}{\hat{L}_s} i_{qc}(k) - T_s\omega_e(k) i_{dc}(k) \\ \quad + \frac{T_s}{\hat{L}_s} u_{qv}(k) - \frac{T_s\omega_e(k)}{\hat{L}_s}\hat{\psi}_f + T_s\hat{f}_q(k) \\ \quad - T_s\gamma_1 \left[\hat{i}_{qc}(k) - i_{qc}(k)\right] \\ z_q(k+1) = z_q(k) - T_s\gamma_2 \left[\hat{i}_{qc}(k) - i_{qc}(k)\right] \\ \hat{f}_q(k+1) = \hat{f}_q(k) - \frac{\omega_o(1-\alpha)}{2\alpha} T_s \left[\hat{f}_q(k) - z_q(k)\right] \\ \quad + \left[G_{rc}(z) + T_s\frac{\gamma_2}{\alpha}\right] \left[i_{qc}(k) - \hat{i}_{qc}(k)\right] \end{cases} \tag{25}$$

where $G_{rc}(z)$ is the discrete form of $G_{rc}(s)$, which can be expressed as

$$G_{rc}(z) = \frac{K_{rc} z^{-N+K}}{1 - Q(z) z^{-N}}. \tag{26}$$

Then, the reference voltage at the k instant with the lumped disturbance compensation based on (6), which can deduced as

$$\begin{bmatrix} u^*_{dv}(k) \\ u^*_{qv}(k) \end{bmatrix} = \hat{P}^{-1} \left\{ \begin{bmatrix} i^*_{dc}(k+2) \\ i^*_{qc}(k+2) \end{bmatrix} - \hat{H}(k) \begin{bmatrix} \hat{i}_{dc}(k+1) \\ \hat{i}_{qc}(k+1) \end{bmatrix} - \hat{M}(k) - T_s \begin{bmatrix} \hat{f}_d(k+1) \\ \hat{f}_q(k+1) \end{bmatrix} \right\}. \tag{27}$$

Accordingly, Fig. 6 presents the whole structure diagram of the proposed DPCC based on the RDCO. The DPCC-RDCO scheme investigated can be divided into three components: disturbance estimation, current prediction, and DPCC controller. The disturbance estimation based on RDCO can achieve the accurate estimation of aperiodic and periodic disturbance $\hat{f}_{dq}(k+1)$. Furthermore, the current prediction utilizes the estimated disturbance to calculate the current $\hat{i}_{dq}(k+1)$ at the next sampling instant. Besides, the DPCC controller with one-sampling delay compensation can obtain the reference voltage based on the estimated disturbance $\hat{f}_{dq}(k+1)$ and the predicted current $\hat{i}_{dq}(k+1)$.

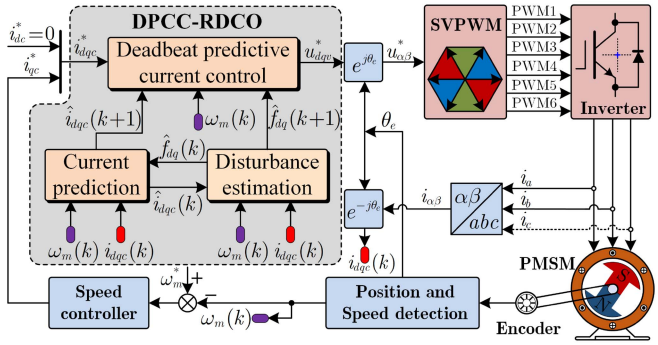

Fig. 6. Structure diagram of the proposed DPCC based on the RDCO.

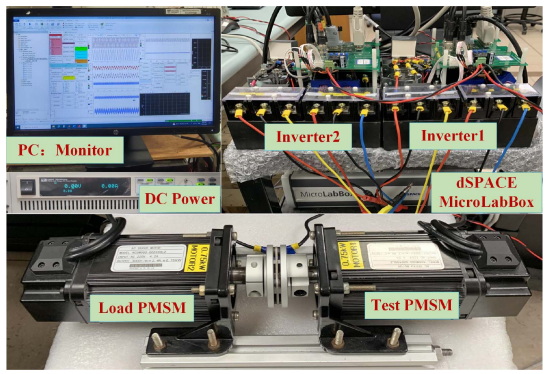

Fig. 7. PMSM test platform.

IV. Experimental Evaluations

A. Experimental Setup

The feasibility and effectiveness of the proposed DPCC-RDCO scheme are comprehensively evaluated experimentally on a PMSM test bench, which is shown in Fig. 7. Meanwhile, the key specifications of the PMSM are summarized in Table I. In this tested bench, the control algorithm is employed on the dSPACE MicroLabBox. The switching frequency of the inverter is 10 kHz and the current sampling period is 100 μs, which ensure that the prediction algorithm is completed within one control cycle. The load PMSM operates in speed mode and the test motor works in current mode to avoid the impact of the speed controller on the verification algorithm.

In order to make a fair comparison between the proposed DPCC-RDCO with DPCC-ESO and DPCC-DCO, the experimental conditions and parameters are consistent. According to the parameter characteristics presented in Section III-B, the appropriate parameters are selected based on trial and error

TABLE I
KEY SPECIFICATIONS OF THE PMSM

Symbols	Parameters	Values	Units
ψ_f	Rotor flux linkage	0.092	Wb
L_s	dq-axis inductance	5.7	mH
R_s	Stator resistance	1.1	Ω
p_n	Pole pairs	4	–
T_L	Rated torque	2.4	N·m
U_N	Rated voltage	220	V
P_N	Rated power	0.75	kW
I_N	Rated current	4.2	A

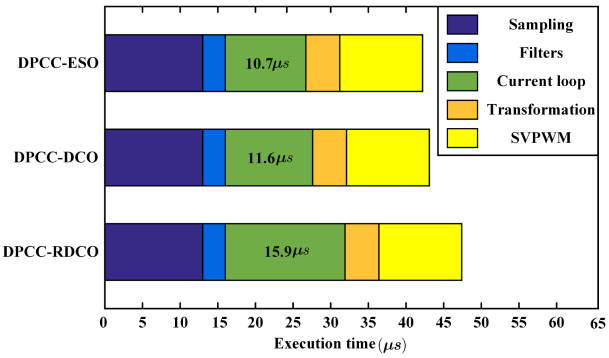

Fig. 8. Comparison of the computational burden of three different methods.

method within a certain parameter range. The parameters of the three observers are set as follows: ω_o=400π, γ_1=2513.3, γ_2=1579136.7, and α=0.4 to achieve low-frequency disturbance correction estimation. The parameters of the repetitive control are selected as follows: K_{rc}=500, $Q(s)$=0.95 [25], and K is typically set as 3 [30]. In addition, the current performance deterioration is more prominent under the low speed and heavy load [12], [23], and [25], so the speed reference is set to 400 r/min in the following experiments.

The comparison of the computational burden of three different control strategies in dSPACE MicroLabBox is shown in Fig. 8. From Fig. 8, the execution times for sampling, filtering, coordinate transformation, and SVPWM are consistent across the three strategies. The DPCC-ESO, DPCC-DCO, and DPCC-RDCO are different current loop control strategies, and their execution times are 10.7, 11.6, and 15.9 μs, respectively. It is observable that the execution times of the proposed DPCC-RDCO and DPCC-DCO are marginally longer than that of DPCC-ESO. Fortunately, the three methods can complete the calculation within a sampling period of 100 μs. Thus, the slight increase in execution time is considered a worthwhile tradeoff for the significant performance improvement achieved with the proposed RDCO approach.

B. Dynamic- and Steady-State Performance Evaluation

In order to compare the dynamic and steady-state performance of the three different DPCC methods, Fig. 9 shows the overall experimental results under rated load. For each subfigure, from top to bottom are the d-axis current, zoomed part of q-axis steady-state current, q-axis current, A-phase zoomed current, A-phase current, and the fast Fourier transform (FFT) results of A-phase zoomed current, respectively. The experimental condition is that the q-axis current reference steps from 5% of the rated current to 100%. With the DPCC-ESO method, there are obvious steady-state fluctuations in the dq-axis currents, with values of 0.993 A and 0.311 A, respectively. The A-phase current has obvious distortion, and its total harmonic distortion (THD) is 6.52%, which is caused by periodic harmonics disturbance. According to the FFT results of phase A current and Table II, the current appears 5th, 7th, 11th, and 13th dominant harmonics, that is, the 6th and 12th harmonics on the dq axis, which is consistent with the theoretical analysis. From Fig. (9(b)), due to the enhanced disturbance estimation and elimination of DPCC-DCO, the dq-axis current ripples and A-phase current distortion are slightly reduced and alleviated. The dq-axis current ripples and the THD of the A-phase current are reduced to 0.781 A, 0.296 A, and 5.37%, respectively. With the proposed DPCC-RDCO, it can be seen that periodic harmonics are effectively attenuated. Specifically, the dq-axis current ripples are 0.325 A and 0.187 A, respectively. The THD of A-phase current decreases to 1.53%, and the amplitudes of each order harmonics are significantly reduced from Table II, and the current sinusoidality is obviously improved.

TABLE II
COMPARISON OF HARMONIC AMPLITUDE UNDER RATED LOAD

Harmonic order	Harmonic amplitude of FFT analysis (%)		
	DPCC-ESO	DPCC-DCO	DPCC-RDCO
5th	5.67	4.78	0.43
7th	2.95	2.63	0.21
11th	1.44	1.35	0.19
13th	1.05	0.96	0.09

Furthermore, the q-axis current dynamic response time is decreased from 4 ms for DPCC-ESO to 2 ms for DPCC-DCO and DPCC-RDCO, and the current dynamic overshoot is also reduced, which is consistent with the analysis in Section III-B. The performance comparison of the three DPCC schemes under rated load is summarized and shown in Fig. 10. It can be seen more intuitively that the DPCC-RDCO solution has lower current fluctuations, less harmonic distortion, and faster dynamic response. In addition, Fig. 11 presents the THD comparison of A-phase current of three different DPCC schemes under different loads. As can be seen, the DPCC-DCO is always slightly better than DPCC-ESO because of its enhanced disturbance estimation, and DPCC-RDCO has the lowest THD and is better than the other two algorithms owing to the repetitive control embedded in it. For example, under 40% rated load, the harmonic distortion of the proposed DPCC-DCO is reduced by 1.5% compared with the DPCC-ESO, while the THD of the studied DPCC-RDCO is decreased by 4.2% compared with the DPCC-DCO. Therefore, the studied DPCC-RDCO has better dynamic performance and stronger disturbance suppression capability, especially in dealing with periodic harmonics.

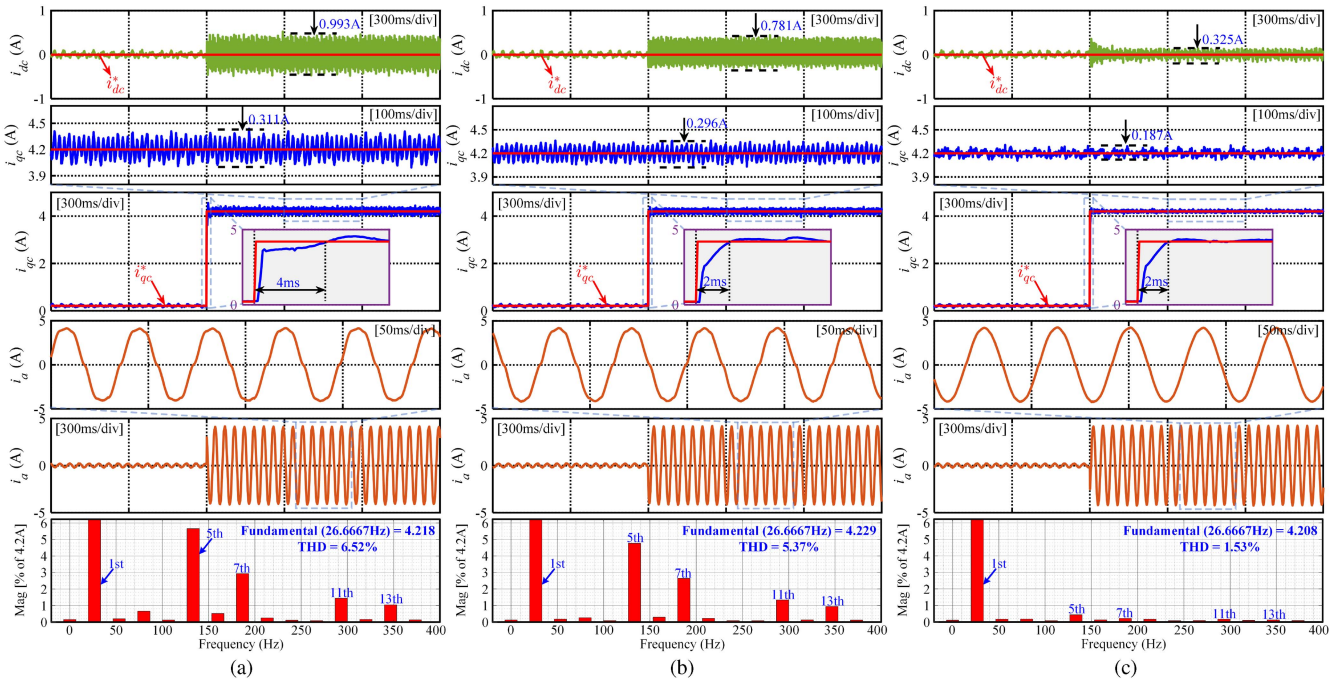

Fig. 9. Experimental results with three different control schemes of the dq-axis current, A-phase current, and its FFT analysis under rated load. (a) DPCC-ESO. (b) DPCC-DCO. (c) DPCC-RDCO.

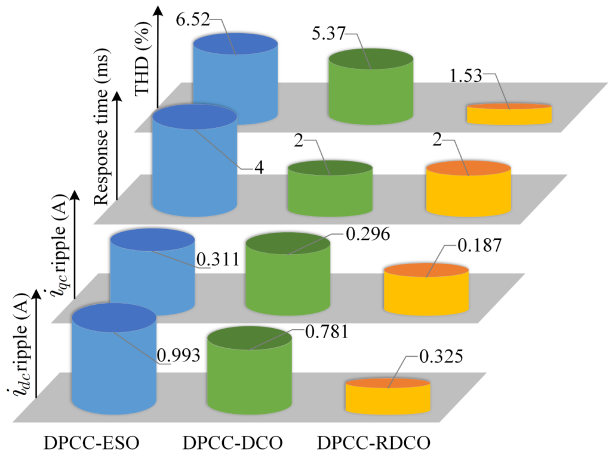

Fig. 10. Performance comparison of three DPCC schemes under rated load.

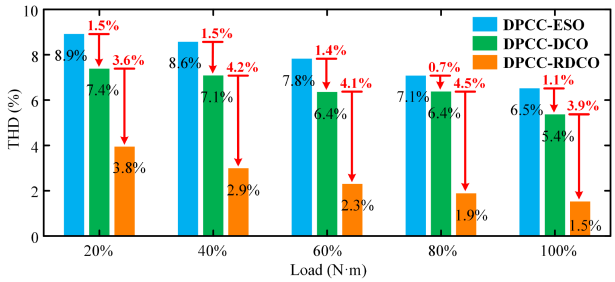

Fig. 11. THD comparison of A-phase current under different loads.

C. Parameter Mismatch Evaluation

In order to evaluate the parameter robustness of three DPCC schemes, Fig. 12 presents the comparison experiment of parameter mismatch under rated load, from top to bottom are the d-axis current, the q-axis current and its zoomed part, and the A-phase current, respectively. It should be noted that PMSM operates without parameter mismatch in the first 0.5 s, and then the flux changes suddenly with $\hat{\psi}_f = 0.5\psi_f$. Then every 1 s interval, the resistance and inductance successively make a sudden variation with $\hat{R}_s = 3R_s$ and $\hat{L}_s = 2L_s$, respectively. In the dynamic characteristics at the moment of parameter mismatch, the q-axis current overshoot of DPCC-ESO is relatively largest (Δe_q: 0.49, 0.93, and 0.54 A), followed by DPCC-DCO (Δe_q: 0.34, 0.38, and 0.35 A), and the smallest is DPCC-RDCO (Δe_q: 0.30, 0.29, and 0.27 A). Moreover, the proposed DPCC-RDCO and DPCC-DCO schemes achieves shorter recovery time (Δt: 8, 6, and 6 ms) compared with DPCC-ESO (Δt: 10, 8, and 8 ms). Compared with the steady-state currents before and after parameter mismatch, the proposed DPCC-RDCO has the smallest current variation (THD before mismatch: 1.53%, THD after mismatch: 1.56%, 1.61%, 1.57%), followed by DPCC-DCO (THD before mismatch: 5.37%, THD after mismatch: 5.39%, 5.58%, 5.47%), and the worst is DPCC-ESO (THD before mismatch: 6.52%, THD after mismatch: 6.43%, 7.29%, 7.11%). The robustness comparisons under parameter mismatch are summarized in Table III.

In order to evaluate the robustness of the proposed method to model parameters that are greater or less than the nominal values, Fig. 13 shows the experimental results of dq-axis current and A-phase current of the proposed DPCC-RDCO with parameter mismatch under rated load. It should be pointed out that the PMSM operates without parameter mismatch in the first

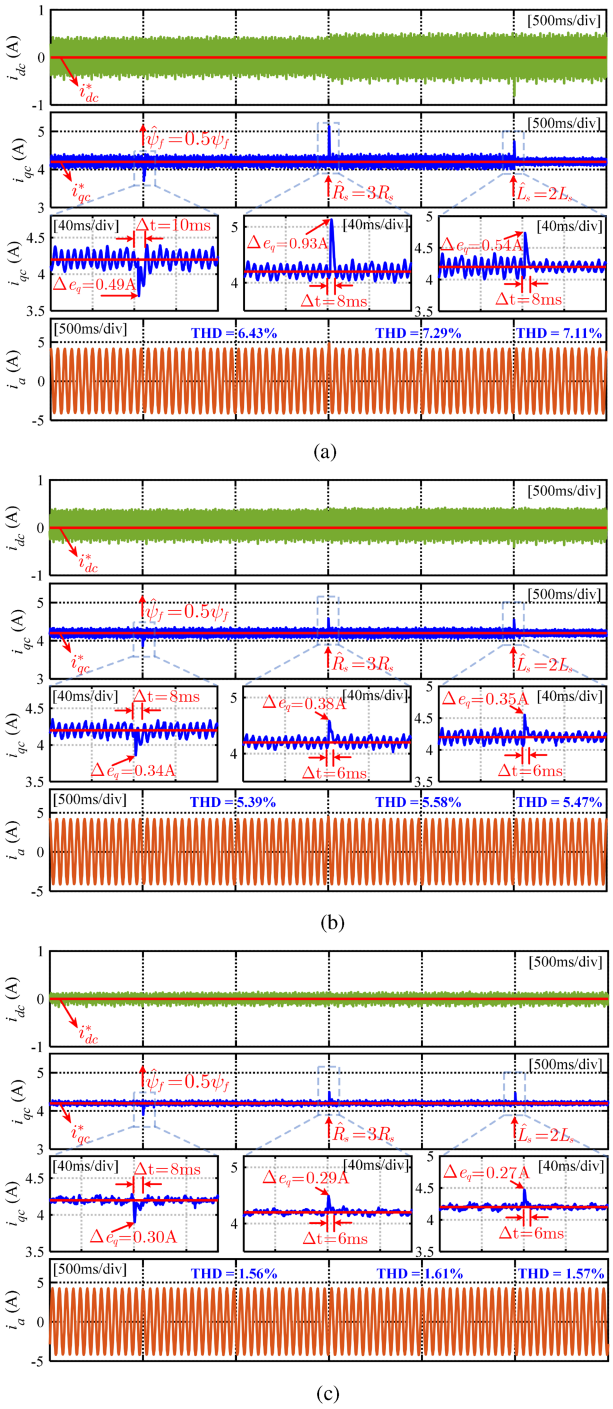

Fig. 12. Experimental results of dq-axis current and A-phase current of three DPCC schemes with parameter mismatch under rated load. (a) DPCC-ESO. (b) DPCC-DCO. (c) DPCC-RDCO.

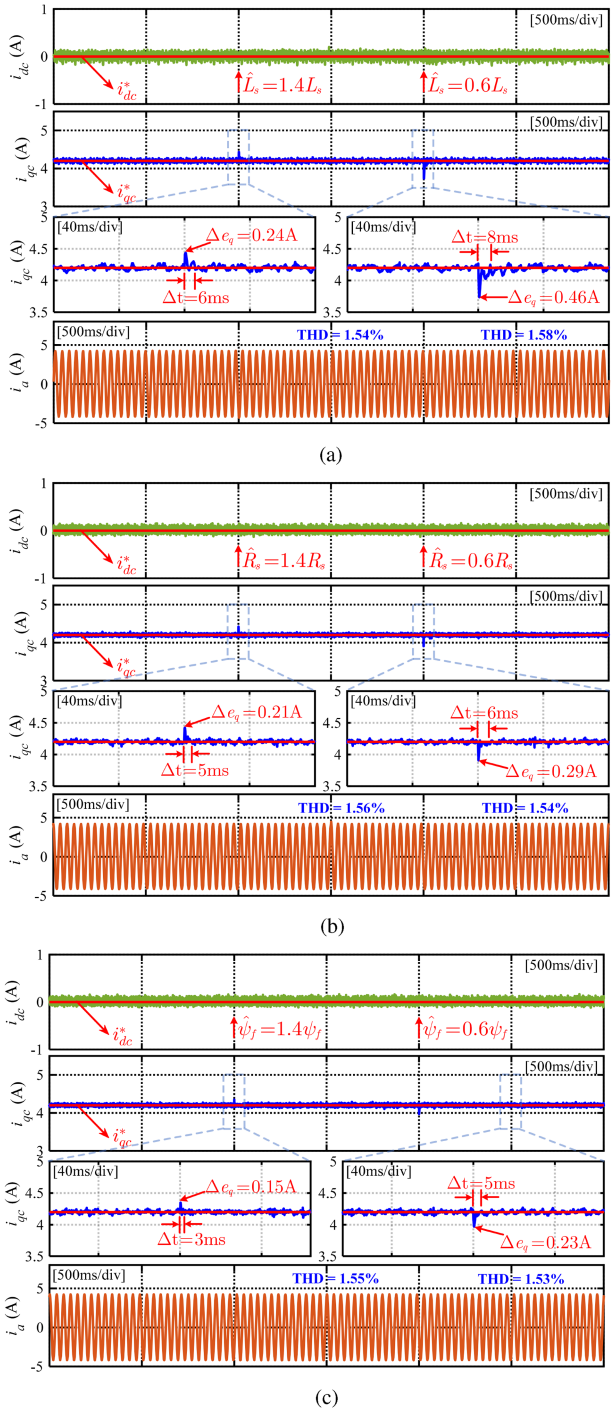

Fig. 13. Experimental results of dq-axis current and A-phase current of the proposed DPCC-RDCO with parameter mismatch under rated load. (a) Inductance mismatch. (b) Resistance mismatch. (c) Flux mismatch.

1 s, and then at every 1 s interval, the inductance, resistance, and flux deviate from the nominal value by 40% upward and downward, respectively. It can be seen from Fig. 13, at the moment of parameter mismatch, the q-axis current has a slight fluctuation, and the fluctuation is quickly eliminated. After the parameter mismatch in the steady state, the mismatch caused by inductance, resistance, and flux linkage causes almost no current change compared to the nominal value parameters. In addition, the phase current THD under the mismatch parameters is still around 1.53% of the nominal value parameters. Thus, it can be concluded that the proposed DPCC-RDCO scheme has excellent robustness to inductance, resistance, and flux mismatch.

To further evaluate the current tracking performance under parameter mismatch, Fig. 14 demonstrates the experimental results of current step and sinusoidal tracking of three DPCC

TABLE III
ROBUSTNESS COMPARISON UNDER PARAMETER MISMATCH

Parameter index		DPCC-ESO	DPCC-DCO	DPCC-RDCO
$\hat{\psi}_f = 0.5\psi_f$	recovery time	10 ms	8 ms	8 ms
	overshoot	0.49 A	0.34 A	0.30 A
	THD	6.43%	5.39%	1.56%
$\hat{R}_s = 3R_s$	recovery time	8 ms	6 ms	6 ms
	overshoot	0.93 A	0.38 A	0.29 A
	THD	7.29%	5.58%	1.61%
$\hat{L}_s = 2L_s$	recovery time	8 ms	6 ms	6 ms
	overshoot	0.54 A	0.32 A	0.27 A
	THD	7.11%	5.47%	1.57%

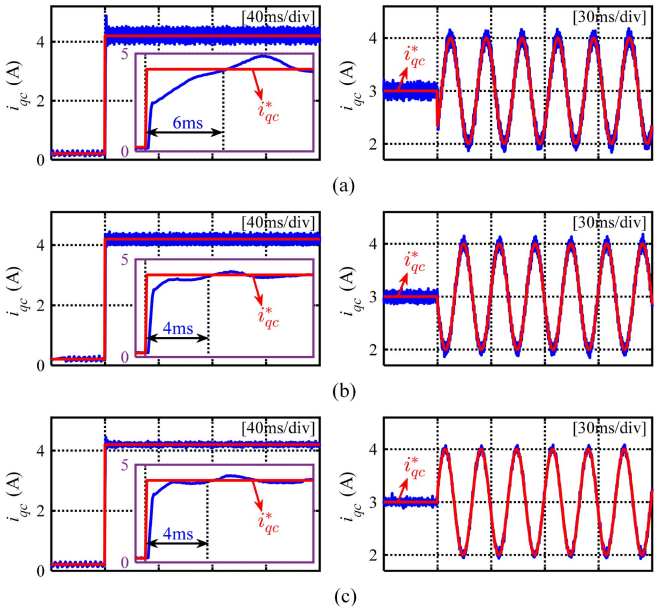

Fig. 14. Current step and sinusoidal tracking experiments of three different DPCC schemes under $\hat{L}_s = 0.7L_s$. (a) DPCC-ESO. (b) DPCC-DCO. (c) DPCC-RDCO.

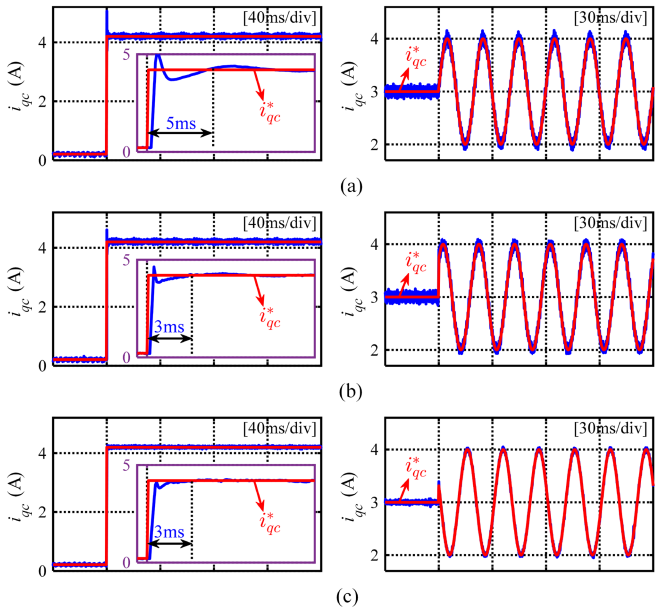

Fig. 15. Current step and sinusoidal tracking experiments of three different DPCC schemes under $\hat{L}_s = 1.3L_s$. (a) DPCC-ESO. (b) DPCC-DCO. (c) DPCC-RDCO.

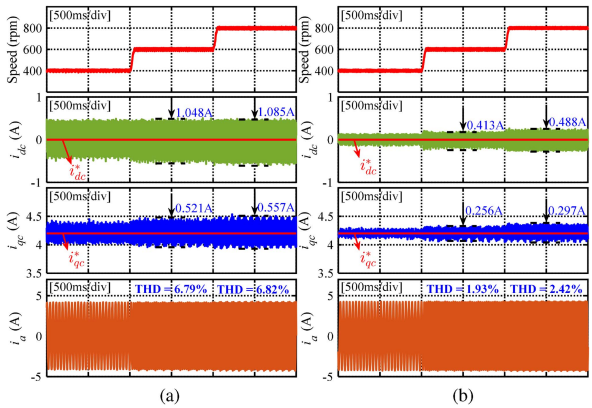

Fig. 16. Experimental results of speed variation under rated load. (a) DPCC-ESO. (b) DPCC-RDCO.

schemes under $\hat{L}_s = 0.7L_s$. The left side of Fig. 14 shows the step from 5% of rated current to 100%. The step time of the three DPCC methods with different disturbance observers is extended by 2 ms compared with the case without mismatch, but the overshoot of the two DPCC methods based on disturbance correction is significantly lower than that of DPCC-ESO, which is also verified that the proposed disturbance correction strategy is more robust. The right side of Fig. 14 presents the tracking $3 + \sin(10\pi)$ sinusoidal current reference. Obviously, the proposed DPCC-RDCO has the smallest tracking error, while the tracking error of DPCC-ESO is relatively large. Fig. 15 presents the current tracking experimental results of three DPCC schemes under $\hat{L}_s = 1.3L_s$, and the similar conclusion as that in Fig. 14 can be obtained. In summary, the investigated DPCC-RDCO has stronger robustness and tracking performance under parameter mismatch.

D. Speed Dynamic Performance Evaluation

Since N in the proposed DPCC-RDCO is calculated in real time based on speed, the performance of the studied strategy should be verified under speed changes. Fig. 16 presents the experimental results of speed changes of DPCC-ESO and DPCC-RDCO under rated load. For each subfigure, from top to bottom are the speed, d-axis current, q-axis current, and A-phase current, respectively. It can be seen that the speed increases from 400 to 600 r/min and then to 800 r/min, and the ripples of dq-axis steady-state current in both control schemes increase, but the ripples of DPCC-RDCO are consistently lower than those of DPCC-ESO. According to the THD analysis of A-phase current, the THD of DPCC-RDCO (1.93%, 2.42%) after the speed increases is significantly lower than that of DPCC-ESO (6.79%, 6.82%), which indicates that the proposed method possesses excellent disturbance suppression performance under

TABLE IV
SPEED VARIATION COMPARISON UNDER RATED LOAD

Parameter index		400 r/min	600 r/min	800 r/min
DPCC-ESO	d-axis ripple	0.993 A	1.048 A	1.085 A
	q-axis ripple	0.311 A	0.521 A	0.557 A
	THD	6.52%	6.79%	6.82%
DPCC-RDCO	d-axis ripple	0.328 A	0.413 A	0.488 A
	q-axis ripple	0.187 A	0.256 A	0.297 A
	THD	1.53%	1.93%	2.42%

speed variation. According to Table IV, it can be found that the proposed RDCO has a better current ripples minimization performance at different speeds. Although the amplitude and frequency characteristics of current harmonic change under variable speed conditions, the proposed DPCC-RDCO based on the repetitive controller is able to adapt the frequency characteristics to effectively suppress current fluctuations in the entire speed range.

V. CONCLUSION

In this article, an improved DPCC with a disturbance correction observer based on repetitive control is proposed to achieve excellent current response and enhance current disturbance suppression performance. Specifically, the disturbance estimation correction is designed to enhance the robustness and the repetitive control is embedded into the disturbance correction term to deal with the periodic harmonics. Meanwhile, the disturbance estimation performance, parameter characteristics, and stability of the proposed observer are theoretically analyzed in detail. The proposed DPCC-RDCO scheme is highly effective in attenuating both aperiodic and periodic disturbances. The experimental results indicate that compared with the basic schemes, the proposed DPCC-RDCO not only minimizes the current errors and harmonics but also maintains steady-state control accuracy and excellent dynamic response, even under parameter mismatch and speed variation conditions. The proposed scheme is potentially achievable to be transplanted to the topological industrial fields.

APPENDIX

The conventional ESO from (7) in the continuous domain can be designed as

$$\begin{cases} \dot{\hat{\boldsymbol{x}}} = \boldsymbol{A}\boldsymbol{x} + \boldsymbol{B}\boldsymbol{u} + \boldsymbol{D} + \hat{\boldsymbol{f}} - \gamma_1(\hat{\boldsymbol{x}} - \boldsymbol{x}) \\ \dot{\hat{\boldsymbol{f}}} = -\gamma_2(\hat{\boldsymbol{x}} - \boldsymbol{x}). \end{cases} \tag{28}$$

The proposed DCO performs disturbance estimation correction on the basis of conventional ESO to enhance the observer robustness, which is constructed as

$$\begin{cases} \dot{\hat{\boldsymbol{x}}} = \boldsymbol{A}\boldsymbol{x} + \boldsymbol{B}\boldsymbol{u} + \boldsymbol{D} + \hat{\boldsymbol{f}} - \gamma_1(\hat{\boldsymbol{x}} - \boldsymbol{x}) \\ \dot{\boldsymbol{z}} = -\gamma_2(\hat{\boldsymbol{x}} - \boldsymbol{x}) \\ \dot{\hat{\boldsymbol{f}}} = \frac{\gamma_2}{\alpha}(\boldsymbol{x} - \hat{\boldsymbol{x}}) - \frac{\omega_o(1-\alpha)}{2\alpha}(\hat{\boldsymbol{f}} - \boldsymbol{z}). \end{cases} \tag{29}$$

REFERENCES

[1] X. Li et al., "A decoupling synchronous control method of two motors for large optical telescope," *IEEE Trans. Ind. Electron.*, vol. 69, no. 12, pp. 13405–13416, Dec. 2022.

[2] H. Cao et al., "Generalized active disturbance rejection with reduced-order vector resonant control for PMSM current disturbances suppression," *IEEE Trans. Power Electron.*, vol. 38, no. 5, pp. 640–6421, May 2023.

[3] Y. Zuo, X. Ge, Y. Zheng, Y. Chen, H. Wang, and A. T. Woldegiorgis, "An adaptive active disturbance rejection control strategy for speed-sensorless induction motor drives," *IEEE Trans. Transport. Electrific.*, vol. 8, no. 3, pp. 3336–3348, Sep. 2022.

[4] T. Yang, Y. Deng, H. Li, Z. Sun, H. Cao, and Z. Wei, "Fast integral terminal sliding mode control with a novel disturbance observer based on iterative learning for speed control of PMSM," *ISA Trans.*, vol. 134, pp. 460–471, 2023.

[5] H. Cao et al., "Unified interpretation of active disturbance rejection control for electrical drives," *IEEE Trans. Circuits Syst. II, Exp. Briefs*, vol. 71, no. 7, pp. 3433–3437, Jul. 2024.

[6] Y. Zhang, J. Jin, and L. Huang, "Model-free predictive current control of PMSM drives based on extended state observer using ultralocal model," *IEEE Trans. Ind. Electron.*, vol. 68, no. 2, pp. 993–1003, Feb. 2021.

[7] Y. A. I. Mohamed and E. F. El-Saadany, "Robust high bandwidth discrete time predictive current control with predictive internal model-a unified approach for voltage-source PWM converters," *IEEE Trans. Power Electron.*, vol. 23, no. 1, pp. 126–136, Jan. 2008.

[8] X. Zhang, B. Hou, and Y. Mei, "Deadbeat predictive current control of permanent-magnet synchronous motors with stator current and disturbance observer," *IEEE Trans. Power Electron.*, vol. 32, no. 5, pp. 3818–3834, May 2017.

[9] P. Cortes, J. Rodriguez, C. Silva, and A. Flores, "Delay compensation in model predictive current control of a three-phase inverter," *IEEE Trans. Ind. Electron.*, vol. 59, no. 2, pp. 1323–1325, Feb. 2012.

[10] S. Dai, J. Wang, Z. Sun, and E. Chong, "Multiple current harmonics suppression for low-inductance PMSM drives with deadbeat predictive current control," *IEEE Trans. Ind. Electron.*, vol. 69, no. 10, pp. 981–9826, Oct. 2022.

[11] C. Xu, Z. Han, and S. Lu, "Deadbeat predictive current control for permanent magnet synchronous machines with closed-form error compensation," *IEEE Trans. Power Electron.*, vol. 35, no. 5, pp. 5018–5030, May 2020.

[12] H. Cao et al., "Improved ADRC with a cascade extended state observer based on quasi-generalized integrator for PMSM current disturbances attenuation," *IEEE Trans. Transp. Electr.*, vol. 10, no. 1, pp. 2145–2157, Mar. 2024.

[13] B. Wang, X. Chen, Y. Yu, G. Wang, and D. Xu, "Robust predictive current control with online disturbance estimation for induction machine drives," *IEEE Trans. Power Electron.*, vol. 32, no. 6, pp. 4663–4674, Jun. 2017.

[14] X. Yuan, S. Xie, J. Chen, S. Zhang, C. Zhang, and C. H. T. Lee, "An enhanced deadbeat predictive current control of SPMSM with linear disturbance observer," *IEEE J. Emerg. Sel. Topics Power Electron.*, vol. 10, no. 5, pp. 6304–6316, Oct. 2022.

[15] X. Gao, M. Abdelrahem, C. M. Hackl, Z. Zhang, and R. Kennel, "Direct predictive speed control with a sliding manifold term for PMSM drives," *IEEE J. Emerg. Sel. Topics Power Electron.*, vol. 8, no. 2, pp. 1258–1267, Jun. 2020.

[16] K. Yu and Z. Wang, "Improved deadbeat predictive current control of dual three-phase variable-flux PMSM drives with composite disturbance observer," *IEEE Trans. Power Electron.*, vol. 37, no. 7, pp. 8310–8321, Jul. 2022.

[17] D. Ke, F. Wang, X. Yu, S. A. Davari, and R. Kennel, "Predictive error model-based enhanced observer for PMSM deadbeat control systems," *IEEE Trans. Ind. Electron.*, vol. 71, no. 3, pp. 2242–2252, Mar. 2024.

[18] Z. Song, F. Zhou, and Z. Zhang, "Parallel-observer-based predictive current control of permanent magnet synchronous machines with reduced switching frequency," *IEEE Trans. Ind. Inform.*, vol. 15, no. 12, pp. 645–6467, Dec. 2019.

[19] O. Babayomi, Z. Zhang, Z. Li, M. L. Heldwein, and J. Rodriguez, "Robust predictive control of grid-connected converters: Sensor noise suppression with parallel-cascade extended state observer," *IEEE Trans. Ind. Electron.*, vol. 71, no. 4, pp. 3728–3740, Apr. 2024.

[20] F. Wang, D. Ke, X. Yu, and D. Huang, "Enhanced predictive model based deadbeat control for PMSM drives using exponential extended state observer," *IEEE Trans. Ind. Electron.*, vol. 69, no. 3, pp. 235–2369, Mar. 2022.

[21] N.-D. Nguyen, N. N. Nam, C. Yoon, and Y. I. Lee, "Speed sensorless model predictive torque control of induction motors using a modified adaptive full-order observer," *IEEE Trans. Ind. Electron.*, vol. 69, no. 6, pp. 6162–6172, Jun. 2022.
[22] A. Bhaumik and S. Das, "Predictive torque control strategy for speed adaptive flux observer based sensorless induction motor drive in flux-weakening region," *IEEE Trans. Power Electron.*, vol. 36, no. 12, pp. 14110–14118, Dec. 2021.
[23] Z. Zhou, C. Xia, Y. Yan, Z. Wang, and T. Shi, "Disturbances attenuation of permanent magnet synchronous motor drives using cascaded predictive integral-resonant controllers," *IEEE Trans. Power Electron.*, vol. 33, no. 2, pp. 1514–1527, Feb. 2018.
[24] J. Lei, S. Fang, D. Huang, and Y. Wang, "Enhanced deadbeat predictive current control for PMSM drives using iterative sliding mode observer," *IEEE Trans. Power Electron.*, vol. 38, no. 11, pp. 13866–13876, Nov. 2023.
[25] M. Tian, B. Wang, Y. Yu, Q. Dong, and D. Xu, "Discrete-time repetitive control-based ADRC for current loop disturbances suppression of IPMSM drives," *IEEE Trans. Ind. Inform.*, vol. 18, no. 5, pp. 3138–3149, May 2022.
[26] Z. Song and F. Zhou, "Observer-based predictive vector-resonant current control of permanent magnet synchronous machines," *IEEE Trans. Power Electron.*, vol. 34, no. 6, pp. 5969–5980, Jun. 2019.
[27] K. Zhou, Y. Yang, F. Blaabjerg, and D. Wang, "Optimal selective harmonic control for power harmonics mitigation," *IEEE Trans. Ind. Electron.*, vol. 62, no. 2, pp. 1220–1230, Feb. 2015.
[28] X. Liu, Y. Deng, J. Wang, H. Li, and H. Cao, "Fixed-time generalized active disturbance rejection with quasi-resonant control for PMSM speed disturbances suppression," *IEEE Trans. Power Electron.*, vol. 39, no. 6, pp. 6903–6918, Jun. 2024, doi: 10.1109/TPEL.2024.3377186.
[29] Z. Gao, "Scaling and bandwidth-parameterization based controller tuning," in *Proc. Amer. Control Conf.*, 2003, pp. 4989–4996.
[30] P. Mattavelli, L. Tubiana, and M. Zigliotto, "Torque-ripple reduction in PM synchronous motor drives using repetitive current control," *IEEE Trans. Power Electron.*, vol. 20, no. 6, pp. 1423–1431, Nov. 2005.

Haiyang Cao (Graduate Student Member, IEEE) was born in Shandong, China, in 1997. He is currently working toward the Ph.D. degree in mechatronic engineering with the University of Chinese Academy of Sciences, Beijing, China, and the Changchun Institute of Optics, Fine Mechanics and Physics, Chinese Academy of Sciences, Changchun, China. Since October 2023, he has been a visiting Ph.D. student with the School of Electrical and Electronic Engineering, Nanyang Technological University, Singapore.

His main research interests include advanced control theories and applications on motor drive systems.

Yongting Deng (Senior Member, IEEE) was born in Shandong, China, in 1987. He received the B.E. degree in automation from the China University of Petroleum (East China), Qingdao, China, in 2010, and the Ph.D. degree in mechatronic engineering from the Changchun Institute of Optics, Fine Mechanics and Physics, Chinese Academy of Sciences, Changchun, China, in 2015.

He is currently a Professor with the Changchun Institute of Optics, Fine Mechanics and Physics, Chinese Academy of Sciences. He has authored or coauthored more than 70 publications in the research interests that include controller design for ac motor drives and linear motor drives, intelligent control, and high-precision machine control techniques.

Jing Liu (Member, IEEE) received the B.E. degree in electrical engineering from the Nanjing University of Aeronautics and Astronautics, Nanjing, China, in 2013, and the Ph.D. degree in mechatronic engineering from the Changchun Institute of Optics, Fine Mechanics and Physics, Chinese Academy of Sciences, Changchun, China, in 2018.

She is currently an Associate Professor with the Changchun Institute of Optics, Fine Mechanics and Physics, Chinese Academy of Sciences. Her research interests include electric machine drives and control techniques.

Yun Zuo (Graduate Student Member, IEEE) received the B.Eng. degree in electrical engineering and automation from Dalian Jiaotong University, Dalian, China, in 2019. He is currently working toward the Ph.D. degree in electrical engineering with Southwest Jiaotong University, Chengdu, China. He is a visiting Ph.D. student with the School of Electrical and Electronic Engineering, Nanyang Technological University, Singapore.

His research interests include ac motor drive systems, sensor fault tolerance, and sensorless control.

Xiufeng Liu (Student Member, IEEE) was born in Changchun, China, in 1998. He received the B.E. degree in vehicle engineering from Changchun University of Technology, Changchun, China, in 2020. He is currently working toward the Ph.D. degree in mechatronic engineering with the University of Chinese Academy of Sciences, Beijing, China, and the Changchun Institute of Optics, Fine Mechanics and Physics, Chinese Academy of Sciences, Changchun, China.

His research interests include ac motor drive, sliding mode control, neural network, and digital control using a digital signal processor.

Huanzhi Wang (Graduate Student Member, IEEE) received the B.Eng. degree in electrical engineering and automation from Dalian Maritime University, Dalian, China, in 2020, and the M.Sc. degree in power engineering from Nanyang Technological University, Singapore, in 2021. He is currently working toward the Ph.D. degree in electrical and electronic engineering with Nanyang Technological University, Singapore.

His research interests include power electronics, electric motor drives, and advanced control strategies.

Christopher H. T. Lee (Senior Member, IEEE) received the B.Eng. (First Class Honours) and Ph.D. degrees both in electrical engineering from Department of Electrical and Electronic Engineering, The University of Hong Kong, Hong Kong, in 2009 and 2016, respectively.

He is currently an Associate Professor with Nanyang Technological University, Singapore. He was a Postdoctoral Fellow and then a Visiting Assistant Professor with Massachusetts Institute of Technology, MA, USA. He is an Associate Editor for IEEE TRANSACTIONS ON INDUSTRIAL ELECTRONICS, IEEE TRANSACTIONS ON ENERGY CONVERSION, IEEE Access, and IET Renewable Power Generation. He is the Chair of IEEE Vehicular Technology Society Singapore Section Chapter in 2023–2025. He is a Chartered Engineer in Hong Kong. His research interests include electric machines and drives, renewable energies, and electromechanical propulsion technologies. In these areas, he has published 2 books, 4 books chapters, and over 270 referred papers.

Dr. Lee was a recipient of the 10th Nagamori Award in 2024, IAS Myron Zucker Student-Faculty Grant in 2023, JSPS Fellowship in 2023, MDPI Energies Young Investigator Award in 2022, NRF Fellowship in 2020, Nanyang Assistant Professorship in 2019, Li Ka Shing Prize (the best Ph.D. thesis prize) in 2017 and Croucher Foundation Fellowship in 2016, and 5 best paper awards, including First Place Best Paper Award in IEEE TRANSACTIONS ON ENERGY CONVERSION in 2022.